Astronomische Nachrichten

Astronomische Nachrichten

ORIGINAL ARTICLE OPEN ACCESS

The Slow-Rotating Nucleus of Comet C/2013 R1 (Lovejoy)

Federico Manzini[1] | Virginio Oldani[1] | Andrea Farina[2] | Paolo Ochner[2,3] | Andrea Reguitti[3,4] | Luigi R. Bedin[3] | Jean Gabriel Bosch[5] | Erik Bryssinck[6] | Roberto Crippa[7] | Stéphan Gaumont-Guay[8] | Carl W. Hergenrother[9] | Joel Nicolas[10] | Ivo Scheggia[11]

[1]Stazione Astronomica di Sozzago, Sozzago (NO), Italy | [2]Department of Physics and Astronomy, University of Padova, Padova, Italy | [3]INAF, Osservatorio Astronomico di Padova, Padova, Italy | [4]INAF, Osservatorio Astronomico di Brera, Italy | [5]Observatoire Chante-Perdrix, Dauban, France | [6]Brixiis Observatory, Kruibeke, Belgium | [7]Osservatorio Astronomico, Tradate (VA), Italy | [8]Chemin du Lac Est, Stoneham, Quebec, Canada | [9]Ascending Node Technologies, LLC, Tucson, Arizona, USA | [10]Vallauris Observatory, Vallauris, France | [11]Osservatorio Monte Lema, Vernate, Switzerland

Correspondence: Luigi R. Bedin (luigi.bedin@inaf.it)

Received: 24 May 2024 | **Revised:** 2 February 2025 | **Accepted:** 12 February 2025

Funding: The authors received no specific funding for this work.

Keywords: inner coma | morphology | solar system: comets (general C/2013 R1)

ABSTRACT

The close approach of comet C/2013 R1 (Lovejoy) allowed us to conduct an in-depth study of the morphology of the inner coma. From the measurement of the dust emission structures expanding near the cometary nucleus in November–December 2013, we derived a slow rotation period of 47.8 ± 1.2 h. The comet's spin axis is oriented approximately at RA = 332° and Dec = +47°. Numerical models of the inner coma suggest that its morphology was related to the presence of at least four main active sources located at different latitudes on the cometary nucleus, emitting dust of relatively small size and with variable velocity.

1 | Introduction

C/2013 R1 (Lovejoy) is a nearly isotropic (long-period) comet discovered on September 7, 2013 (CBET 3649; Howes et al. 2013). It does not appear to be a dynamically new comet (Combi et al. 2018), with an estimated orbital period of nearly 12,000 years (Small-Body Database Lookup). Comet Lovejoy reached perihelion on December 22.7, 2013, at a distance of 0.81 AU. It follows a 64° inclined and highly eccentric orbit ($e = 0.998$). Observations of the inner coma with different filters showed a complex morphology, probably due to the presence of several active regions on the nucleus (Opitom et al. 2015). To date, no data has been published on the rotation period and pole position of comet C/2013 R1 during its passage in 2013. Therefore, the aim of our work was to characterize the details of the inner coma and to analyze the changes in its morphology over a period of approximately 4 months around perihelion, in order to determine the spin axis orientation and the rotation period of the comet's nucleus.

2 | Image Collection and Processing

We followed the passage of comet C/2013 R1 for about 4 months between November 9, 2013, and March 3, 2014, thus spanning a long period before and after the perihelion date, and collected good quality CCD images useful for the analyses described in this paper, taken with different telescopes or retrieved from public archives, on 32 observational nights.

Each night, the images were taken over a time span of no more than 30 min to ensure that the details in the inner coma were not blurred by rotation. The images were then calibrated with standard procedures and co-added to maximize the

TABLE 1 | List of images used and astrometry data.

Date	Telescope	Resolution (km/pixel)	Filter	RA (°)	Dec (°)	*r* (AU)	Delta (AU)	Sun PA (°)	STO (°)	Axis PA (°)	Axis incl. (°)
2013-Nov-09	B96	851	Clear	134.84	21.37	1.144	0.487	106	60	−12.3	20.1
2013-Nov-12	290	122	*R*	142.50	26.43	1.108	0.446	108	63	−6.6	16.3
2013-Nov-13	B96	759	Clear	145.50	28.21	1.096	0.434	109	65	−4.5	14.8
2013-Nov-15	B96	727	Clear	152.24	31.82	1.072	0.416	112	67	0.3	11.4
2013-Nov-21	GG	837	Clear	178.49	40.74	1.006	0.398	126	76	18.8	−1.8
2013-Nov-28	B51	314	*R*	211.52	42.35	0.936	0.451	148	83	37.7	−13.9
2013-Dec-02	T09	74	*R*	225.58	39.98	0.901	0.508	157	84	44.0	−18.8
2013-Dec-03	A12	259	Clear	228.45	39.24	0.894	0.524	159	84	45.0	−19.8
2013-Dec-03	T09	76	*R*	228.45	39.24	0.894	0.524	159	84	45.0	−19.8
2013-Dec-04	T09	78	*R*	231.09	38.47	0.886	0.541	160	84	46.0	−20.7
2013-Dec-04	A12	267	*R*	231.09	38.47	0.886	0.541	160	84	46.0	−20.7
2013-Dec-05	A12	276	*R*	233.52	37.69	0.879	0.559	161	83	46.7	−21.6
2013-Dec-06	A12	284	Clear	235.76	36.90	0.872	0.577	162	83	47.4	−22.3
2013-Dec-07	A12	293	*R*	237.82	36.11	0.865	0.595	163	83	47.9	−23.0
2013-Dec-08	B13	339	*R*	239.72	35.33	0.859	0.614	164	82	48.3	−23.7
2013-Dec-10	Lema	274	*R*	243.11	33.79	0.847	0.652	165	81	48.9	−24.7
2013-Dec-11	Lema	283	*R*	244.62	33.04	0.842	0.672	165	80	49.1	−25.2
2013-Dec-12	Lema	291	*R*	246.02	32.30	0.837	0.692	166	80	49.2	−25.6
2013-Dec-13	Lema	299	*R*	247.33	31.58	0.833	0.712	166	79	49.3	−26.0
2013-Dec-14	Lema	308	*R*	248.55	30.87	0.829	0.732	166	78	49.3	−26.3
2013-Dec-15	Lema	316	*R*	249.69	30.18	0.825	0.752	166	77	49.3	−26.6
2013-Dec-17	A12	391	*R*	251.77	28.83	0.819	0.792	165	75	49.2	−27.1
2013-Dec-27	A12	488	*R*	259.36	22.87	0.816	0.990	160	65	47.8	−28.3
2014-Jan-01	OAO/NAOJ	1193	*R*	262.07	20.26	0.831	1.082	156	60	46.8	−28.4
2014-Jan-06	OAO/NAOJ	1287	*R*	264.38	17.85	0.856	1.167	151	56	45.8	−28.3
2014-Jan-12	Lema	530	*R*	266.77	15.20	0.898	1.260	144	51	44.7	−28.0
2014-Jan-13	Lema	536	*R*	267.14	14.78	0.906	1.274	143	50	44.5	−28.0
2014-Jan-21	OAO/NAOJ	1517	*R*	269.83	11.65	0.980	1.376	134	46	42.9	−27.5
2014-Jan-26	OAO/NAOJ	1576	*R*	271.31	9.88	1.033	1.429	128	44	42.0	−27.2
2014-Jan-29	290	397	*R*	272.13	8.88	1.067	1.457	125	43	41.5	−27.0
2014-Jan-30	OAO/NAOJ	1616	*R*	272.40	8.56	1.078	1.466	124	42	41.4	−26.9
2014-Feb-11	OAO/NAOJ	1703	*R*	275.15	5.02	1.225	1.545	112	40	39.5	−26.0
2014-Mar-01	W96	796	Clear	277.80	0.53	1.462	1.590	99	38	37.4	−24.1
2014-Mar-03	OAO/NAOJ	1753	*R*	277.97	0.06	1.489	1.590	98	37	37.2	−23.9

Note: Observatory codes: B96 Brixiis Observatory, Kruibeke, 0.4 m (Belgium); 290 VATT 1.83 m (AZ, USA); GG Quebec City, lat. +46.997° long. 71.390°, 0.1 m (Canada); B51 Vallauris, 0.4 m (France); B13 Osservatorio di Tradate, 0.65 m (Italy); A12 Stazione Astronomica di Sozzago, 0.4 m (Italy); T09 Subaru Telescope, Maunakea, 8.0 m (Hawaii); OAO/NAOJ lat. +34.573° long. 133.597°, 0.5 m (Japan); Lema lat. +46.041° long. −8.838°, 0.4 m (Switzerland); W96 CAO, San Pedro de Atacama, 0.4 m (Mexico). RA, Dec, *r*, Delta, Sun PA, STO have been taken from the NASA/JPL web app Horizons System (https://ssd.jpl.nasa.gov/horizons/). Axis PAs and Inclinations are computed according to the estimated coordinates of the comet's pole. Perihelion date was December 22.7, 2013.

signal-to-noise ratio. The full list of images, by date and with a description of their characteristics, is shown in Table 1.

The vast majority of the images used for our analysis were taken with *R*-band filter, which is widely used to study dust emissions and prevent gas contamination. For example, (Hasegawa and Kawakita 2017) used only the *R*-band images for their analysis of the dust emissions, in order to prevent contamination from gas (on the assumption that gas is an optically thin, spherically symmetric, radially expanding outflow). In addition, in their research they isolated CN and C3 gas emissions from dust emission by subtracting the scaled *R*-band images from those taken with the narrowband filters.

The comparison of the *BVR* composite of three images taken with the Johnson *B*, *V* and *R* filters on December 11, 2013, with the

67/92-cm Schmidt telescope at the INAF-OAPd-Asiago Astrophysical Observatory, with the image taken in the *R*-band after processing with the Larson-Sekanina filter (alpha = 20°), showed that the morphological structures near the nucleus were superimposable, demonstrating that they derived essentially from dust emissions. In fact, the dust components (*R* band) were grouped in the same active areas with a minimal gas component (*V* and *B* band) (Figure 1).

The jet-like structures observed in the inner coma of comet R1 extended for thousands of kilometers, and their shape was visibly affected by the solar gravity and radiation pressure, which suggests that at those distances they were composed mainly (if not solely) of dust. Despite the potential gas contamination, the few images taken without filters showed the same morphological details as the *R*-filtered images (Figure 1), therefore they were considered useful for our analysis, in particular to support the development of a synthetic model of the inner coma throughout all of the observation dates.

All the calibrated images were subjected to further processing with different digital filters to highlight the possible presence of radial features (i.e., dust jets) and/or haloes (i.e., shells), which are barely distinguishable from the surrounding

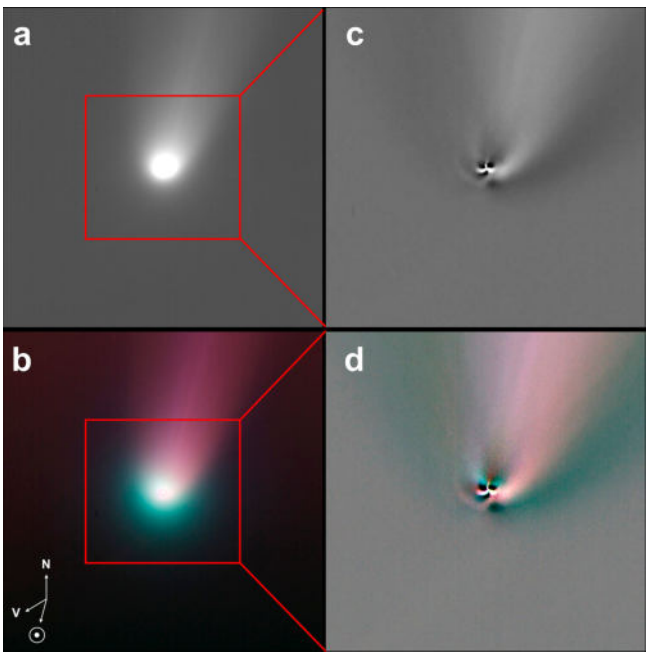

FIGURE 1 | Images taken on December 11, 2013, with the 67/92-cm Schmidt telescope (INAF-OAPd-Asiago Astrophysical Obs.). (a) *R*-band image. (b) *BVR* composite: The coma appears spherical and isotropic, the green color is due to C2 emissions in the wavelength of the *V* band. The tail is reddened by scattering of sunlight by dust. (c) and (d) the Larson-Sekanina filter (alpha = 30°) has been applied to the images of panels a and b. The structures near the nucleus are superimposable, showing that they essentially derive from dust emissions. Panel d shows how the dust components (*R*-band) are grouped in the same active areas with a minimal gas component (*V*- and *B*-band). A green gaseous emission is observed from an active area. Field of view in panels a and b is 348 arcsec equivalent to 169,200 km at the distance of the comet from Earth on that date. The images in panels c and d are upscaled 2×.

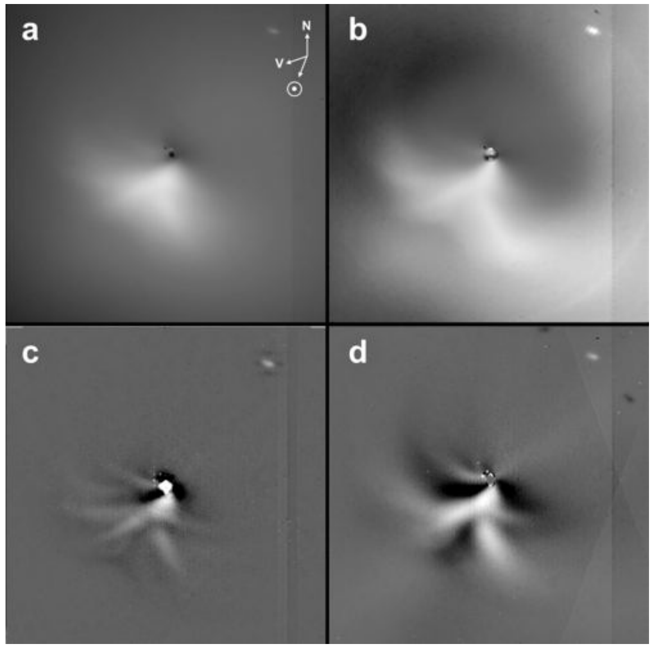

FIGURE 2 | Comparison of the processing of the same image with four digital filters. (a) $1/\rho^{0.7}$; (b) Azimuthal Renormalization; (c) Radially Variable Spatial Filtering; (d) Larson-Sekanina ($\alpha = 20°$). All filters show the same features, although the Larson-Sekanina returns the greatest detail and contrast. Image taken with the 8-m SUBARU telescope on December 3, 2013. North is up. The field of view of each square box is 80 arcsec, equivalent to 30,400 km at the distance of the comet from Earth on that date.

brightness within the inner coma in unprocessed images. Among the different filters used, the Larson-Sekanina spatial filter (Larson and Sekanina 1984), applying a rotational shift of 20° to avoid ghosts and artifacts, returned the most detailed results. An extensive comparison with other digital filters: $1/\rho$, $1/\rho^{0.7}$, Azimuthal Renormalization and Radially Variable Spatial Filtering (Samarasinha et al. 2014), substantially confirmed the findings. The results are shown in Figure 2. These latter filters allowed us to identify the presence of the same structures in the same images, but with a lower contrast than the aforementioned Larson-Sekanina treatment which, for this reason, was the preferred choice for our analyses.

3 | Estimate of the Gas-To-Dust Ratio in the R-Band

We performed a specific analysis in order to confirm that the structures examined in the inner coma of C/2013 R1 were mainly composed of dust, in order to be able to carry out a numerical modeling and identify the main parameters characterizing the activity on the nucleus of the comet.

The abundance of dust emissions in the inner coma, compared to a limited presence of gases, on images taken in the R-band, is confirmed in Figure 3a, which show the three bandwidths of the *B*, *V*, *R* Johnson filters superimposed on a spectrum of the comet taken on November 26, 2013 (Credits: Christian Buil https://buil.astrosurf.com/comet/lovejoy/obs.htm). The spectrum appears

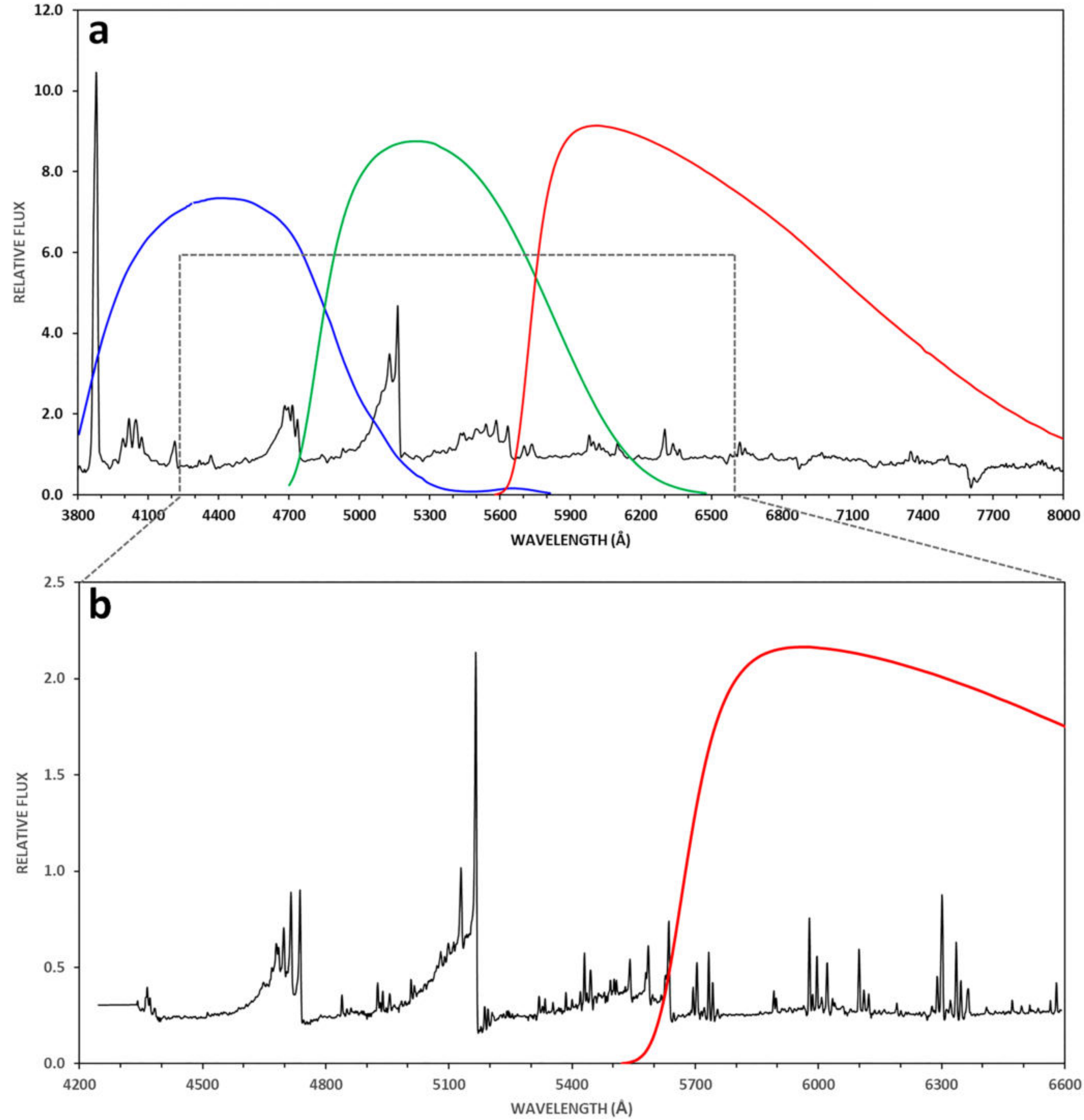

FIGURE 3 | The three bandwidths of the Johnson B, V, R filters are superimposed on a spectrum of comet Lovejoy of November 26, 2013, taken with a 0.28 m telescope at the Castanet Observatory in France (a). The spectrum appears almost "clean" from the presence of the major emissions of known gases (CN, C2, C3, NH, NH2) in the R filter bandwidth. (b) The bandwidth of the R filter is superimposed on a spectrum of the comet taken on November 29, 2013, with the 1.2-m Galileo Telescope at the Asiago Astrophysical Observatory, extending on a narrower wavelength range (indicated by the dotted line on the spectrum in panel a).

in fact almost "clean" from the major emissions of known gases (CN, C2, C3, NH, NH2) in the R filter bandwidth.

To determine the gas-to-dust ratio in the R-filtered images, we used a medium-resolution spectrum of comet Lovejoy taken on November 29, 2013, with the 1.2-m Galileo Telescope at the Asiago Astrophysical Observatory, equipped with a grating of 600 lines/mm (200 μm slit aperture—dispersion 1.18 Å/pixel) (Figure 3b). The wavelength range in this spectrum extends from 4246 to 6592 Å: since the bandwidth of the R filter starts at 5500 Å, the range considered to calculate the gas-to-dust ratio was limited between 5500 Å and the maximum extension of the spectrum toward red. For a proper flux calibration, Hamuy et al. (1994) ESO Standard Star HR3454 was used; to remove the solar contribution, the cometary spectrum was calibrated with a spectrum (taken in the same observing session) of the star

Hyades64, which is a solar analogue. The IRAF v2.6 software was used for the reduction of the spectrum, with the standard calibration for dark, bias signal and flat field. Wavelength calibration was performed using He-Fe-Ar lamps. The spectrum was analyzed by estimating in the *R* bandwidth the continuum, assumed as due to the dominant contribution of dust, and calculating the net contribution of gas based on the fluxes of all the identified emission lines (e.g., C2, NH2). The continuum was estimated as median value between the considered wavelengths, and the net gas flow was calculated by subtracting the estimated continuum from the total flux. The resulting total percentage of gas was 9.3% ± 1.9%. This value can be considered valid not only for the spectral range analyzed, but also for the entire extension of the *R* bandwidth, because beyond the reading limit set for our analysis there are no significant emissions, and the spectrum appears to be almost continuous (Figure 3b).

To confirm these results, an analysis was also performed on the spectrum of the comet of November 26, 2013, taken with an Alpy 600 spectrograph (23 μm slit) on a 0.28-m f/6.5 telescope, which extends from 3800 to 8000 Å (Figure 3a). The analysis, conducted with the same method as above, resulted in a gas contribution of 9.2% ± 1.9%, a value comparable to that previously estimated.

4 | Determination of the Comet's Rotation Period

The images enhanced with the spatial filters revealed shell-like features resulting from dust emissions expanding from a rotating nucleus (Sekanina and Larson 1984), most evident in the south-east quadrant, between the position angles (PA) 90° and 180°. Nearly matching morphology, offset by a small amount, was seen in numerous pairs of images, which showed a repetitive pattern about every two consecutive days.

We collected data on 18 observational nights, often consecutive, over a period of 38 days before perihelion (from November 9 to December 17, 2013) to confirm these observations. To standardize the measurements of the details in the inner coma of the comet and the comparisons between dates, the stacked images were scaled to the same resolution of approximately 300 km/pixel and rotated according to the comet's sky motion angle as seen from Earth. Each processed image was submitted to polar coordinates transformation centered on the optocenter (i.e., the assumed position of the nucleus), with the θ angle on the horizontal axis and the distance from the optocenter, in pixels, on the vertical axis. Subsequently, photometry was measured on the polar-transformed images on a vertical line parallel to the distance axis at a position corresponding to PA 120° (i.e., where the "shells" appeared most evident), the highest luminosity corresponding to the distance of the features from the nucleus, projected on the sky-plane, on each date (Figure 4). The measurements have an estimated error of ±1.5 pixels. To account for the changing viewing geometry from Earth on the observing interval, all the measurements were corrected for the cosine of the inclination of the spin axis on the plane of the sky, calculated for each date according to the found coordinates of the pole as described in Section 5. The corrected distances were then plotted and, on the assumption that the morphology varied at a constant rate (i.e., that it resulted from a constant rotation speed of the nucleus), a least square fit of a sinusoidal model to the data was drawn according to the following function:

$$y = a + b \cdot \sin(2\pi \cdot c \cdot (t + d)) \tag{1}$$

where a = midpoint, b = amplitude, c = frequency (i.e., number of rotations/day), t = time in JD and d = phase. The best fitting curve resulted in a frequency $c = 0.5017$, corresponding to a rotation period of 47.8 ± 1.2 h (Figure 5). We also evaluated sub-multiple fractions of this period, but without finding suitable solutions.

During the observation period between November and December 2013, the shells into the second and third quadrants (south of the nucleus) showed an expansion modulated by a clockwise rotation, so as per convention, the cometary nucleus was facing the Earth with its south pole (an animation is available in the Supporting Information).

5 | The Active Areas

The morphology of the inner coma of comet Lovejoy (Figure 6) appeared extraordinarily complex, with the simultaneous presence of shells, haloes, fans and jets, probably originating from several active sources on the nucleus. A detailed analysis on the CCD images of the characteristics of the inner coma and of their evolution due the rotation of the nucleus and to the effects of radiation pressure on the dust emissions related to the variations in the Sun-comet geometry during the movement of the comet

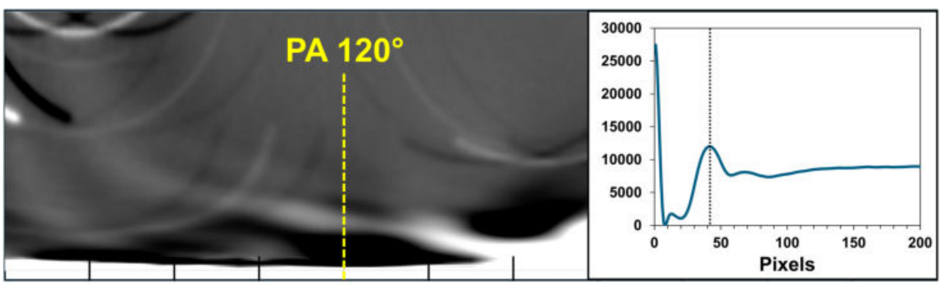

FIGURE 4 | Image of December 8, 2013, transformed to polar coordinates centered on the optocenter. The θ angle (PA) is on the horizontal axis and the distance from the optocenter, in pixels, is on the vertical axis. The shell is well visible. Photometry is measured on a vertical line parallel to the distance axis at PA 120°. The curve on the right shows the peak luminosity corresponding to the distance in pixels of the shell from the nucleus, projected on the sky-plane.

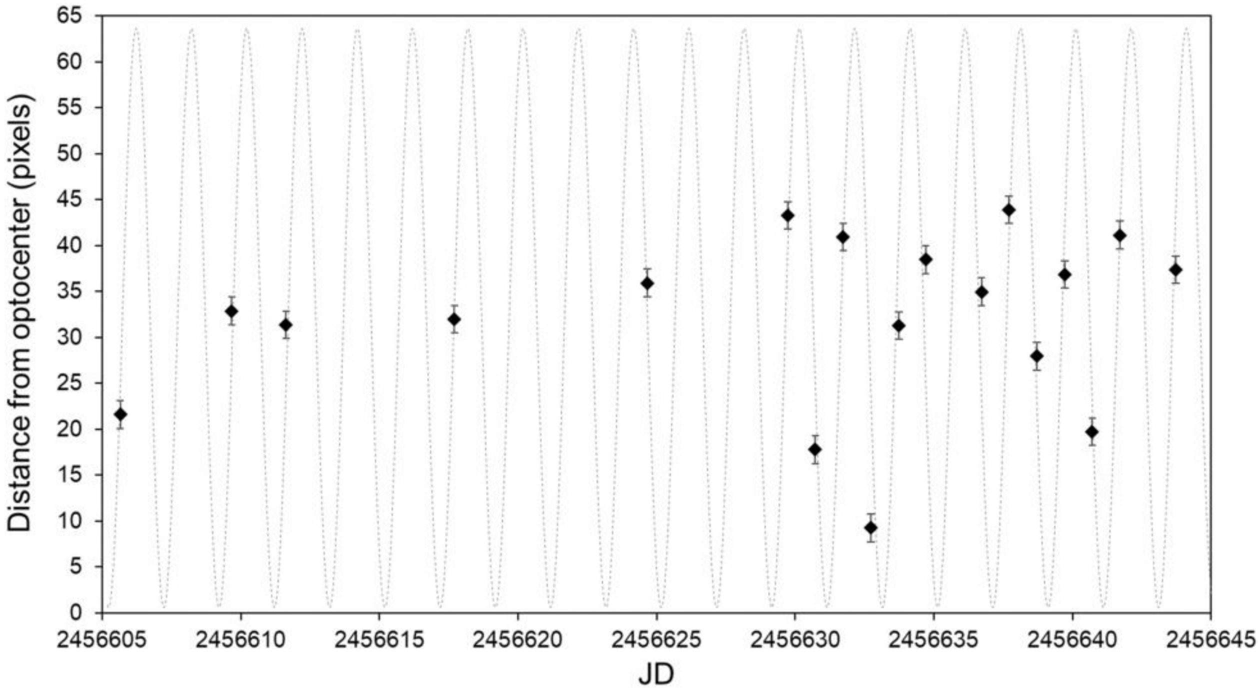

FIGURE 5 | Plot of the distances in pixels of the shells from the optocenter (black diamonds, ± S.E.), measured at PA = 120° and corrected for the inclination of the spin axis on the sky plane for each date. The best fit of a sinusoidal model (period = 47.8 h) to the data is shown as a dotted line. JD 2456610 = 2013-11-14; JD 6640 = 2013-12-14.

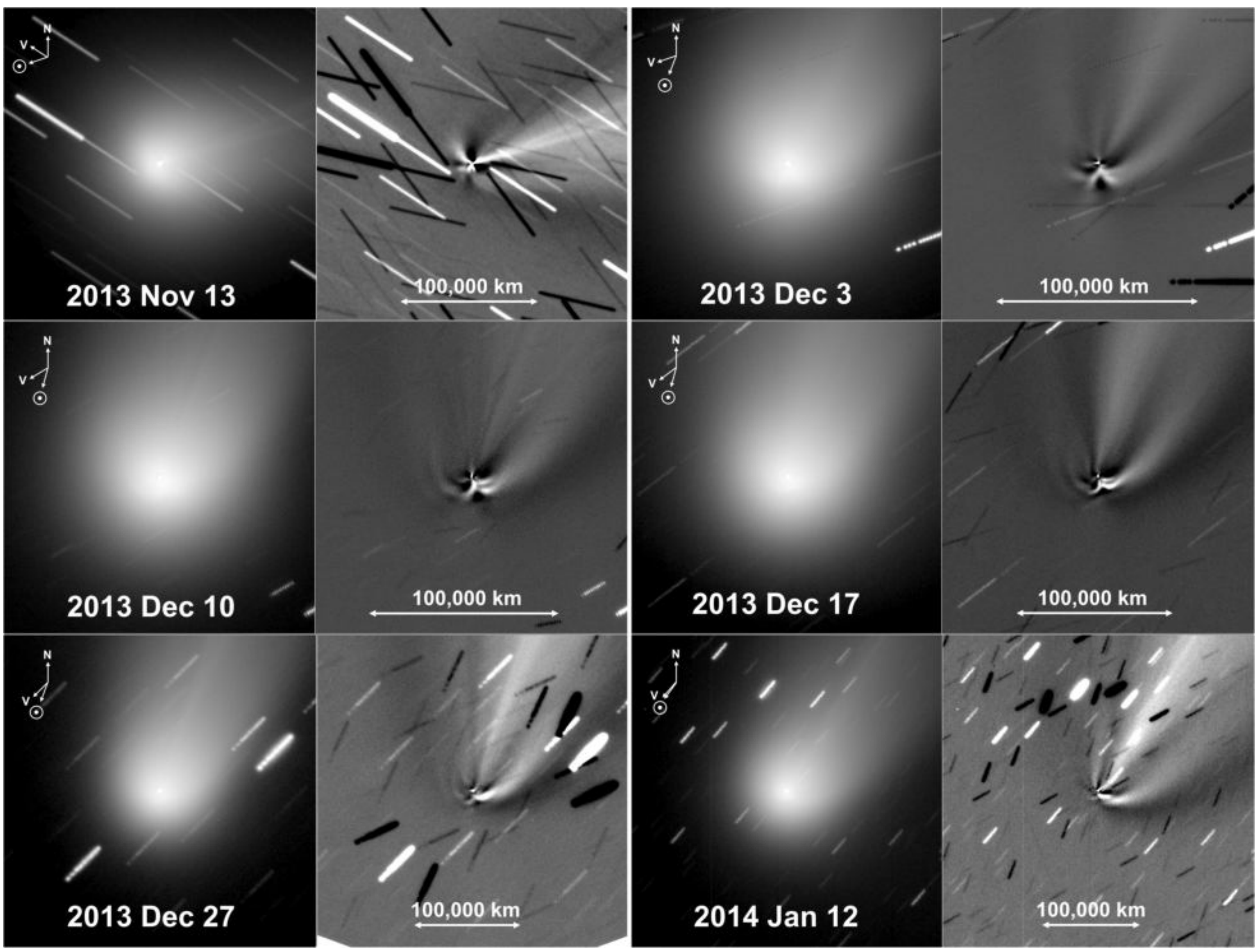

FIGURE 6 | Images of the inner coma of comet Lovejoy taken on different dates before and after perihelion are shown together with the corresponding processing with the Larson-Sekanina filter, which highlights the details of the dust jets. See Table 1 for details of each image.

along its orbit, as well as the changing view from Earth, allowed us to attribute the complex morphology to the presence of at least four discrete sources at different latitudes on the nucleus surface.

A numerical modeling of the inner coma features observed on the processed CCD images was run for each date using our proprietary software *FASE 6*, specifically designed to provide a bi-dimensional graphical representation of Earth-based observations of the dust coma structures, based on the rotating jet model (details on the modeling process can be found in Manzini et al. 2021). The models derive from calculations based on the Finson–Probstein equation (Finson and Probstein 1968), which analyzes the motion of dust emitted by a cometary nucleus and subject to the action of solar gravity and radiation pressure according to the appropriate geometry data (image scale in km computed according to the comet-Earth distance Delta and to the resolution of the telescope, comet-Sun distance r, Sun PA and phase angle STO) once they have been entered into the software.

The modeling process followed a trial-and-test approach: the initial model parameters (number and location of the active sources, dust size and density, dust emission velocity, orientation of the spin axis) were developed on the high-resolution images of early December 2013 taken with the Subaru 8-m telescope, when the comet was at a distance of only 0.52 AU from Earth and 0.89 AU from the Sun. The resulting draft models were assessed by superimposing them on the CCD images and varying their transparency to allow a direct comparison with the coma features. The software parameters were then adjusted one by one in small steps until a satisfactory match was obtained.

The final parameters found on these high-resolution images were then applied backward until November 9 (comet at 0.49 AU from Earth and 1.14 AU from the Sun) and forward to March 3, 2014 (comet at 1.59 AU from Earth and 1.49 AU from the Sun) by changing only the geometry data and the orientation of the spin axis computed for each date based on the estimated coordinates of the comet's pole (see Section 5 and Table 1), and proved to be consistently correct across the entire observation period. Examples of the resulting modeling of the inner coma structures, alongside the original CCD images processed with the Larson-Sekanina filter ($\alpha = 20^{\circ}$) are shown in Figure 7. The dust emission models obtained were highly reproducible placing four active areas at the following latitudes on an assumed spherical nucleus:

- J1: -68°; the jet-like emission from this area was the most prominent and constant feature in the majority of the images and was taken as the main reference for the parameters of the model.
- J2: -15°.
- J3: $+15^{\circ}$.
- J4: $+30^{\circ}$.

The latitude position of the active areas can be considered accurate with an error of $\pm 3^{\circ}$, beyond which significant differences arise between the models and the images. We used fixed arbitrary longitudes, as the available data did not allow to constrain the longitude of the active regions.

The dust particle size that produced models that best matched the morphological structures observed on the images according to the Finson–Probstein equations, was between 1.2 and 10 μm, assuming a grain density of $1.0\ \mathrm{gcm^{-3}}$, and between 2.4 and 20 μm assuming a grain density of $0.5\ \mathrm{gcm^{-3}}$, for corresponding β values between 0.1 and 1. These particle diameters were inversely related to dust emission velocities between 120 and $360\ \mathrm{ms^{-1}}$ for the jet-like emissions from the active areas J1 and J4, and between 180 and $540\ \mathrm{ms^{-1}}$ for the low-latitude structures J2 and J3, indicating a possible broad distribution of the dust particle size within the anisotropic emissions. Dust particles with diameter or density outside those ranges did not produce results comparable to the images.

The emission velocities not only appeared to be different between the four active areas, being lower in the low latitude areas J1 and J4 and higher in the higher latitude areas J2 and J3, but also to vary with the heliocentric distance, particularly in the two latter areas (Figure 8).

The parameters used in the modeling process (or their effectiveness ranges), together with error estimate (where applicable) are summarized in Table 2.

6 | Determination of the Spin Axis Orientation

The spin axis orientation was sought using a trial-and-test approach, by systematically varying by few degrees its position angle (PA) and inclination on the plane of the sky, over the simulated comet's nucleus—assumed spherical—in the modeling software, until a graphical representation of the features that best matched with those observed on the CCD images in all the observation dates was produced (some examples are shown in Figure 7).

Successively, we estimated with the least square (LSQ) method the RA and Dec coordinates of the comet's pole as those that provided computed PAs and inclinations of the spin axis that best fitted those adopted in the numerical models, by minimizing the sum of the squares of the O-C. The PAs and inclinations (I) of the spin axis were computed for each date according to the following formulas:

$$\mathrm{PA}\,(^{\circ}) = \arctan\left[\frac{\cos\delta_p \cdot \sin(\alpha_p - \alpha_{\mathrm{com}})}{\cos\delta_{\mathrm{com}} \cdot \sin\delta_p - \sin\delta_{\mathrm{com}} \cdot \cos\delta_p \cdot \cos(\alpha_p - \alpha_{\mathrm{com}})}\right] \tag{2}$$

$$I\,(^{\circ}) = \arccos\left(\cos(\alpha_p - \alpha_{\mathrm{com}}) \cdot \cos\delta_{\mathrm{com}} \cdot \cos\delta_p + \sin\delta_{\mathrm{com}} \cdot \sin\delta_p\right) - 90^{\circ} \tag{3}$$

where α_{com}, δ_{com} are the RA and Dec coordinates (in decimal degrees) of the comet for a given date (see Table 1) and α_p, δ_p are the estimated RA and Dec coordinates of the comet's pole.

The minimization returned values of the O-C $< 1^{\circ}$ in most of the observation dates, with a total RMS error of 0.7° for the PAs and of 1.1° for the inclination angles, the relevant fitting curves resulting from a best estimate of the α_p, δ_p parameters (i.e., the coordinates of the pole) at RA = 331.8° and Dec = +46.8°.

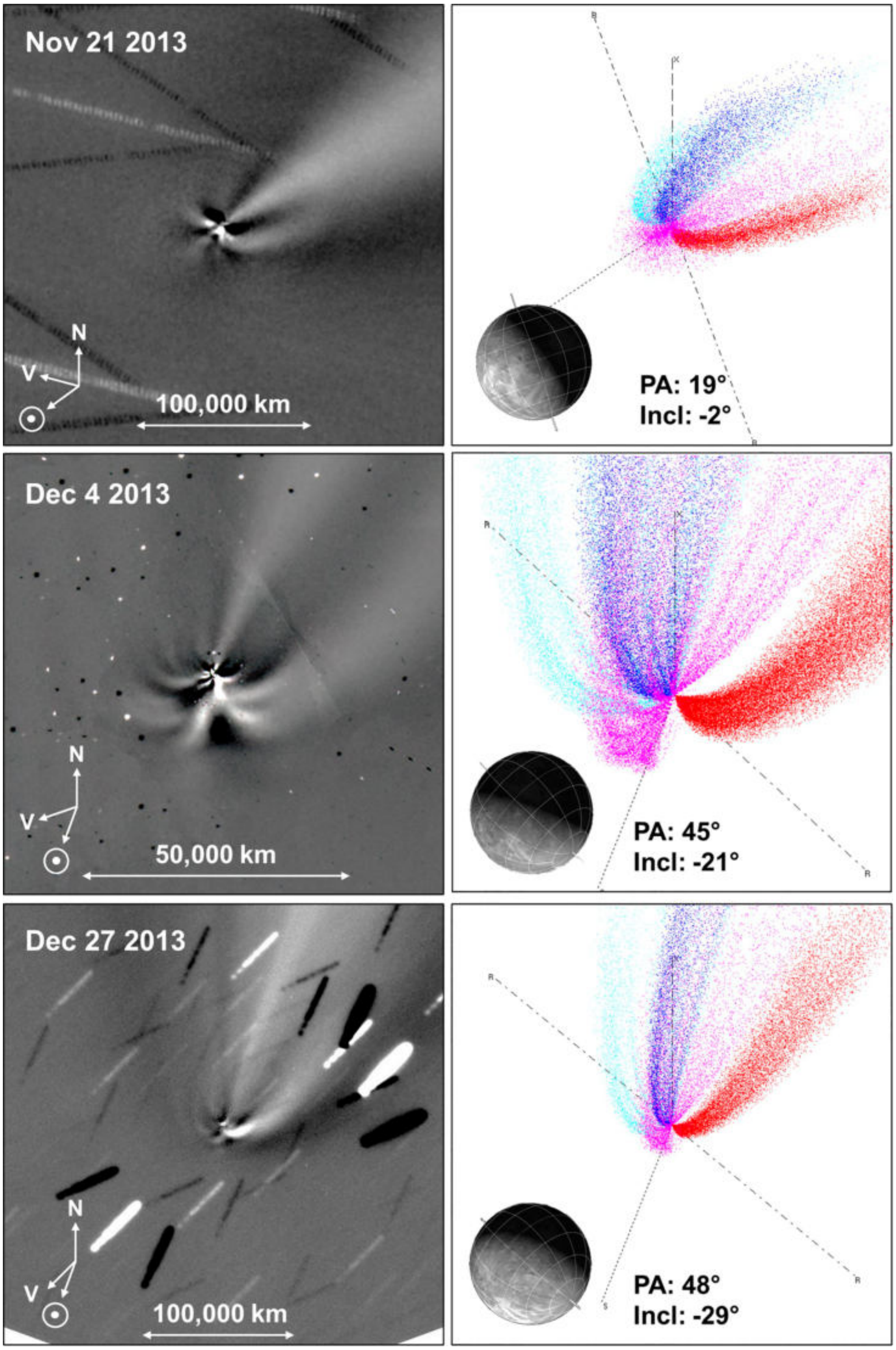

FIGURE 7 | Examples of modeling of the inner coma structures. Left: Original CCD image processed with the Larson-Sekanina filter ($\alpha = 20^{\circ}$). Right: numerical model, drawn according to the found parameters of spin axis position, rotation period, number and location of the active sources, dust particle size and emission velocity. The different colors indicate the emissions from the four sources identified (red: latitude -68°, blue: latitude $+30^{\circ}$, violet: latitude -15°, cyan: latitude $+15^{\circ}$). A graphical representation of the nucleus, with the spin axis orientation and the extent of insolation as seen from Earth is also shown.

The error ellipse of this estimate of the pole coordinates is comprised between RA = 329.6° to 332.2° and Dec = 43.7° to 49.8°, assuming a position error of $\pm 3^{\circ}$ for both the PAs and the inclinations entered in the numerical models.

Furthermore, graphical simulations of the viewing geometry of the comet's nucleus, always assumed spherical, were compared with the images taken on the same dates in order to verify that the physical parameters set for the nucleus in the modeling

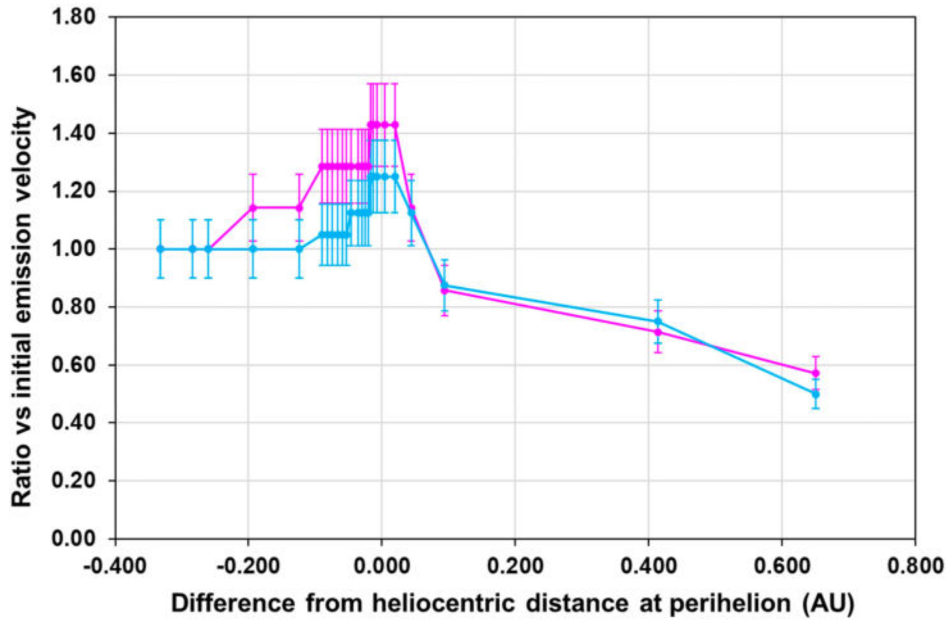

FIGURE 8 | Variations of the emission velocity in the low-latitude active areas (−15°, cyan and +15°, violet) as a function of the heliocentric distance. The variations (±10% estimation error) are shown as ratio versus the initial velocity throughout the observation period. The heliocentric distance is shown as difference from that at perihelion (occurred on December 22.7, 2013), indicated by 0.000 AU.

TABLE 2 | Parameters used in the modeling process.

Latitude of active areas	J1: −68° (±3°) J2: −15° (±3°) J3: +15° (±3°) J4: +30° (±3°)
Dust emission velocity	J1, J4: 120–360 m s^{-1} J2, J3: 180–540 m s^{-1}
Dust particle diameter and density	2.4–20.0 μm—density 0.5 g cm^{-3} 1.2–10.0 μm—density 1.0 g cm^{-3}

software (in particular, the estimated direction of the spin axis and the extent and amount of insolation of the active areas) were compatible with the morphologic features visible in the images (Figures 7 and 9). Accurate graphical simulations were obtained with the software Starry Night 8.1 Pro (Simulation Curriculum Corp., Minnetonka (MN), USA).

7 | Discussion

The physical characteristics of the nucleus of C/2013 R1 appear rather peculiar, including a slow rotation, a high number of active sources on the surface, probably emitting dust of different sizes and with different velocities. In addition, it was found to show CO-rich gas emissions (Paganini et al. 2014).

The rotation period of comet C/2013 R1, determined in 47.8 ± 1.2 h, places its nucleus among those with an "extremely slow" rotation: of the 60 comets whose period is known (Knight et al. 2023), only five are described with a slower rotation. For 15 long-period comets listed in the same paper, the rotation period has already been determined, and they all have nuclei with a faster rotation than that of comet Lovejoy, with the exception of C/1983 H1 (IRAS-Araki-Alcock) and C/2014 S2 (PanStarrs).

Our numerical models of the dust emissions showed that, within the limitations of the modeling process (mainly that the jets are emitted normal to a spherical surface and composed of only one size of dust particles at a time), they agree well with the CCD images by imposing a dust particle diameter between 1.2 and 20 μm for a density of 0.5–1.0 gcm^{-3}. The size of the dust particles found from our models is in agreement with the size of the "grains" that constitute the dust and dust aggregates coming from the emissions of comet 67P and observed with the COSIMA instrument on the Rosetta probe (ESA) (Bentley et al. 2016; Mannel et al. 2016). From the analysis of the dust particles collected by COSIMA around perihelion and before and after the equinoxes, (Merouane et al. 2017) observed a different size distribution between the two hemispheres of comet 67P, which suggested possible differences in the nature of the terrains in the two hemispheres of the comet. Without any constraints on the two parameters—diameter and density—we cannot infer the exact distribution of the dust characteristics or to confirm whether the four sources emitted dust particles of different sizes; however, since most of the images were taken with the *R* filter, we can assume that the size of the optically important grains is mostly within the estimated ranges, and that the corresponding true emission velocities are also probably within the estimated ranges of 120–540 ms^{-1}.

The emission velocities showed variable values depending on the latitude of the active sources, higher for the sources at low latitudes +15° and −15°, and lower for the sources at higher latitudes +30° and −68°. It could be that different illumination levels or seasonal effects determined different dust production rates in the four active areas, and consequently also affected the relevant emission velocities. These findings seem in agreement with the

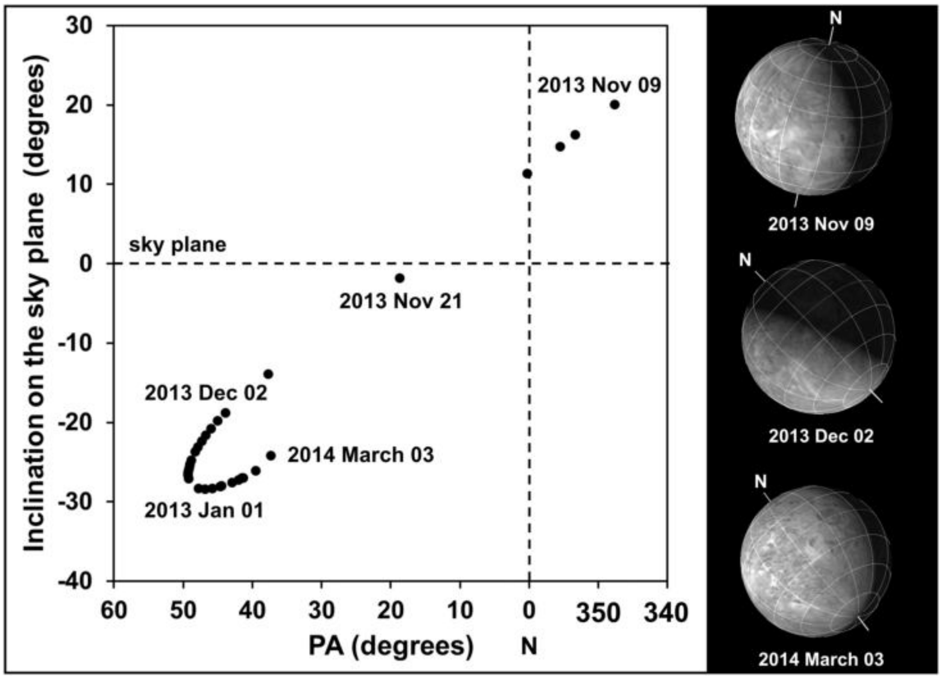

FIGURE 9 | Left: apparent motion of comet's Lovejoy pole as PA and inclination on the sky plane as seen from Earth during the observation period. The horizontal dashed line is the sky plane; dots with positive inclination values indicate the pole is directed toward Earth while those with negative inclination values indicate the pole is directed away from Earth. The vertical dashed line indicates North. The North pole of the spin axis moved toward East and farther behind the sky plane until the perihelion date (December 22.7, 2013), then it inverted its motion. Right: graphical simulation of the orientation of the spin axis and of the extent of insolation of the nucleus as seen from Earth at the beginning, middle and end of the observation period.

observations of (Opitom et al. 2015), who reported that the radicals analyzed in the coma of comet Lovejoy may not all come from the same source and that the mix of ice and dust was probably different in the various active areas. However, we would be cautious about this claim as we have no evidence for this, although (Läuter et al. 2022) found characteristic differences in the surface ice composition for the two hemispheres of comet 67P.

The emission velocities found with our modeling appear not only different between the four sources, but also to vary as a function of the heliocentric distance (Figure 8). The trend shown in the figure is consistent with the observations by (Merouane et al. 2017), who found a variability of the dust flux on comet 67P depending on the distance of the comet from the Sun. In particular, they observed the maximum flux at perihelion in terms of number of particles, but before perihelion in terms of mass, and concluded that the dust particles collected by COSIMA before perihelion were larger than those collected after perihelion. The data provided by (Moreno 2022) also contributes to demonstrating that the physical properties of the particles, the size distribution and the ejection speeds vary with the heliocentric distance.

The orbit followed by the comet and the orientation of the spin axis at RA = 332° and Dec = +47° entailed that the four active sources, if observed from the Sun, were in a position to receive solar radiation during the entire period of the perihelion passage: none of them have ever been in full darkness. Models produced with the found direction of the spin-axis show that at the time of perihelion the south pole was facing the Sun, with the spin axis tilted only about +30° onto the plane of the sky as seen from there. All the active sources therefore were hit by solar radiation for at least half rotation of the nucleus (about 24 h). These conditions remained unchanged throughout the observation period, thus favoring an almost continuous emission from all sources, only modulated by rotation of the nucleus.

Since no phenomena related to rapid precession have ever been observed, the direction of the spin axis can be considered as invariant in the short run.

8 | Conclusions

Analysis of the morphology of the inner coma on high-resolution images of comet C/2013 R1 (Lovejoy) collected on 32 dates between November 9, 2013, and March 3, 2014, allowed us to find:

- At least four main active areas on the nucleus;
- Different dust emission velocities in the four active areas;
- Variable emission velocities as a function of the heliocentric distance;
- A rotation period of the nucleus of about 48 h;
- An orientation of the spin axis in equatorial coordinates approximately at RA = 332°; Dec = +47°;
- An invariant direction of the spin axis through the observation period;
- The analysis of two spectra allowed to estimate at 9.3% ± 1.9% the mean contribution of gases within the

wavelength of the Johnson *R* filter, thus confirming that the observed jet-like features were composed mainly of dust.

The following Supporting Information is available as part of the online article:

- GIF animated images:
  - C2013-R1-20131203-to-15-ls20.gif
  - C2013-R1-20131203-to-15-ls20-polar.gif

The images collected between December 3 and December 15, 2013 were aligned on the cometary nucleus and stacked in groups to create six composite images referring to the respective observation nights. These images were then scaled to the same resolution of 300 km/pixel and rotated according to the comet's sky motion angle as seen from Earth. A Larson-Sekanina spatial filter ($\alpha = 20^\circ$) and a polar projection centered at the optocenter were then applied.

Finally, the images rendered in an animation phased on the rotation period found, show the motion of the structures observed in the inner coma.

Acknowledgments

This work is partially based on data collected at the Subaru Telescope and Okayama Astrophysical Observatory, and obtained from the SMOKA archive, which is operated by the Astronomy Data Center, National Astronomical Observatory of Japan (NAOJ), and on observations with the VATT: the Alice P. Lennon Telescope and the Thomas J. Bannan Astrophysics Facility. This research is based also on observations collected at the Schmidt telescope (Asiago, Italy) of the INAF—Osservatorio Astronomico di Padova; the images are directly downloadable from the INAF institutional archive interface. We thank Edoardo Radice for sharing his early work on the modeling of this comet. We are grateful to Christian Buil for having made his comet spectra available to the community. We wish to thank the anonymous referee for the valuable comments and suggestions. Open access publishing facilitated by Istituto nazionale di astrofisica, as part of the Wiley - CRUI-CARE agreement.

Conflicts of Interest

The authors declare no conflicts of interest.

References

Bentley, M. S., R. Schmied, T. Mannel, et al. 2016. "Aggregate Dust Particles at Comet 67P/Churyumov-Gerasimenko." *Nature* 537, no. 7618: 73–75.

Combi, M. R., T. T. Mäkinen, J. L. Bertaux, et al. 2018. "Water Production Activity of Nine Long-Period Comets From SOHO/SWAN Observations of Hydrogen Lyman-Alpha: 2013–2016." *Icarus* 300: 33–46.

Finson, M. L., and R. F. Probstein. 1968. "A Theory of Dust Comets. I. Model and Equations." *Astrophysical Journal* 154: 327–352.

Hamuy, M., N. B. Suntzeff, S. R. Heathcote, A. R. Walker, P. Gigoux, and M. M. Phillips. 1994. "Southern Spectrophotometric Standards. II." *Publications of the Astronomical Society of the Pacific* 106: 566.

Hasegawa, T., and H. Kawakita. 2017. "The Abel Transformation Deconvolves Comets: Gas Structure of Comet C/2013 R1 (Lovejoy)." *Publications of the Astronomical Society of Japan* 69, no. 3: 54.

Howes, N., H. Sato, T. Lister, et al. 2013. "Comet C/2013 R1 (Lovejoy)." *Central Bureau Electronic Telegrams* 3649: 1.

Knight, M. M., R. Kokotanekova, and N. H. Samarasinha. 2023. "Physical and Surface Properties of Comet Nuclei From Remote Observations." arXiv e-prints arXiv:2304.09309.

Larson, S. M., and Z. Sekanina. 1984. "Coma Morphology and Dust-Emission Pattern of Periodic Comet Halley. I—High-Resolution Images Taken at Mount Wilson in 1910." *Astronomical Journal* 89: 571–578.

Läuter, M., T. Kramer, M. Rubin, and K. Altwegg. 2022. "The Ice Composition Close to the Surface of Comet 67P/Churyumov-Gerasimenko." *ACS Earth and Space Chemistry* 6, no. 5: 1189–1203.

Mannel, T., M. S. Bentley, R. Schmied, et al. 2016. "Fractal Cometary Dust—A Window Into the Early Solar System." *Monthly Notices of the Royal Astronomical Society* 462: S304–S311.

Manzini, F., V. Oldani, P. Ochner, et al. 2021. "Coma Morphology and Dust Emission Pattern of Comet C/2020 F3 (NEOWISE)." *Monthly Notices of the Royal Astronomical Society* 506, no. 4: 6195–6202.

Merouane, S., O. Stenzel, M. Hilchenbach, et al. 2017. "Evolution of the Physical Properties of Dust and Cometary Dust Activity From 67P/Churyumov-Gerasimenko Measured In Situ by Rosetta/COSIMA." *Monthly Notices of the Royal Astronomical Society* 469: S459–S474.

Moreno, F. 2022. "Monte Carlo Models of Comet Dust Tails Observed From the Ground." *Universe* 8, no. 7: 366.

Opitom, C., E. Jehin, J. Manfroid, D. Hutsemékers, M. Gillon, and P. Magain. 2015. "TRAPPIST Photometry and Imaging Monitoring of Comet C/2013 R1 (Lovejoy): Implications for the Origin of Daughter Species." *Astronomy & Astrophysics* 584: A121.

Paganini, L., M. J. Mumma, G. L. Villanueva, et al. 2014. "C/2013 R1 (Lovejoy) at IR Wavelengths and the Variability of CO Abundances Among Oort Cloud Comets." *Astrophysical Journal* 791, no. 2: 122.

Samarasinha, N., P. Martin, and S. Larson. 2014. Cometary Coma Image Enhancement Facility. http://cie.psi.edu.

Sekanina, Z., and S. M. Larson. 1984. "Coma Morphology and Dust-Emission Pattern of Periodic Comet Halley. II—Nucleus Spin Vector and Modeling of Major Dust Features in 1910." *Astronomical Journal* 89: 1408–1425.

Supporting Information

Additional supporting information can be found online in the Supporting Information section.